# Rotating Scatter Mask Optimization for Gamma Source Direction Identification

**Darren E. Holland[a], James E. Bevins[b], Larry W. Burggraf[b], Buckley E. O'Day[b]**

[a] Department of Mechanical Engineering
Cedarville University
Cedarville, OH 45502 USA
[b] Department of Engineering Physics
Air Force Institute of Technology
Wright-Patterson AFB, OH

## 1 Abstract

**Rotating scattering masks have shown promise as an inexpensive, lightweight method with a large field-of-view for identifying the direction of a gamma emitting source or sources. However, further examination of the current rotating scattering mask design shows that the identification could be improved to reduce or eliminate degenerate solutions and improve required count times by changing the geometry. These changes should produce more linearly independent characteristics for the mask, resulting in a decrease in the mis-identification probability. Three approaches are introduced to generate alternative mask geometries. The eigenvector method uses a spring-mass system to create a geometry basis. The binary approach uses ones and zeros to represent the geometry with many possible combinations allowing for additional design flexibility. Finally, a Hadamard matrix is modified to examine a decoupled geometric solution. Four criteria are proposed for evaluating these methodologies. An analysis of the resulting detector response matrices demonstrates that these methodologies produced superior identification characteristics than the original design. The eigenvector approach produces the least linearly dependent results, but exhibits a decrease in average efficiency. The binary results are more linearly dependent than the eigenvector approach, but this design achieves a higher average efficiency than than original. The Hadamard-based method produced a lower maximum, but a higher average linear dependence than the original design. Further possible design enhancements are discussed.**

## 2 Introduction

Identifying a gamma source's direction is important in a variety of applications such as providing security, treaty compliance verification, and locating orphan sources. Three general categories exist for gamma source direction identification; count-based systems, collimator and coded aperture systems, and Compton cameras. A novel, alternative approach, similar in concept to the coded aperture system, exists that eliminates many of the limitations of alternative approaches. This system utilizes a mask placed over a single position-insensitive detector [1]. The system records energy spectra as a function of the geometrically varying mask, which is accomplished through a set, constant rotation of the mask. The position dependent spectra obtained, referred to as detector response curves (DRCs), depend on the source position and can be used to identify the source direction. FitzGerald's mask geometry results in some DRCs that are nearly identical, which can lead to mis-identification of the source direction. This work seeks to reduce the DRCs' linear dependence by optimizing the mask's geometry.

FitzGerald introduced the RSM that has a 14 inch diameter and surrounds a 3 x 3 inch cylindrical NaI scintillating detector [1]. His original MCNP model contained 31 elements or one element every 11.6°. In order to increase the accuracy of the geometric representations, the model's angular resolution was later increased to every degree.

FitzGerald's design methodology assumes that the detector response is related to the mask geometry. Without this assumption, intentional mask design degenerates into random trial and error. In addition, he proposed three desirable characteristics for the RSM system. First, for any given initial source position, there is a unique response curve generated as the mask rotates 360°. This condition is necessary as a non-unique response would make at least two initial source position DRCs indistinguishable and a unique identification impossible.

## 3 RSM Design

Logan et al. [2] showed statistical agreement between experimental and simulated DRCs using GEANT4 [3] and simulated to simulated DRCs using GEANT4 and MCNP [4]. Thus, this work will use MCNP to simulate the experimental DRCs needed for evaluating each RSM design's performance. Instead of using only the full energy peak (FEP), the DRC for this work is formed by summing all counts above 200keV to increase the source direction identification's efficiency. The 200keV limit was chosen as Logan et al. noted discrepancies for counts below this value due to scatter in the environmental elements not considered in the model [2].

Originally, both the analysis of FitzGerald's RSM and the new designs were to be discretized into 10° increments in $\theta$ and 5° in $\phi$. However, due to requirements for the Hadamard method, (which is discussed in Section 3.3.3) the proposed designs are broken into 32 discrete angles in $\theta$ resulting in $\Delta\theta = 11.25°$ and $\Delta\phi = 5.625°$ for 30 angles in $\phi$.

The RSM design is to be optimized for a $^{137}$Cs point source located 36 inches from the center of the detector, mimicking Logan et. al's setup [2]. To simulate the relative source rotation in MCNP, the mask is stationary, while the source is rotated in spherical coordinates every degree for $\theta$ from 0 to 348.75° and for each $\phi$ from 5.625° to 168.75°. The modeled NaI detector includes a 1/8 inch 2024 Aluminum alloy sleeve on which the acrylic RSM is placed. The maximum width of the RSM depends on the methodology, but the maximum mask thickness is a constant 7.87 inches (20 cm). A sphere of air surrounds the source and detector,

and all other environmental factors were ignored. To increase the solution convergence rate, particles were emitted within a 27.26° half angle cone extending from the source to the detector's center. This variance reduction technique assumes that the effect of the few particles that scatter in the air outside of the cone, though the mask, and into the detector will have negligible contributions to the simulated DRCs. In addition, a 0.095 inch air gap between the mask and aluminum sleeve constrains the mask geometry from impinging on the sleeve and provides a space for grease to be applied between the moving parts. Finally, due to manufacturing constraints, each mask angle must have a non-zero thickness.

### 3.1 Design Assumptions and Limitations

To best enable source direction identification, a unique set of DRCs must be obtained. The complete set of DRCs for all rotations angles forms the design response matrix (DRM). The primary criterion for the design choice will be the design with the most unique DRM.

For this application, it is desirable that the curve generated at each initial source position be orthogonal - a.k.a. unique - to the others. Let this curve be denoted $\mathbf{DRC}_{i,j}$, where $i = 0,1,...,n$ is the initial $\theta$ and $j = 0,1,...,m$ is the initial $\phi$ index relative to a reference location on the mask. Since the mask rotates, the $i^{th}$ DRC will be identical to the $g^{th}$ DRC shifted by $g-i$ indices. A negative number corresponds to a shift to the left and a positive number a shift to the right. This property greatly impacts the mask design as any periodic vector with respect to $\theta$ will then result in duplicate $i$ and $g$ DRCs. The duplication due to periodicity would fail to meet the design's uniqueness requirements.

### 3.2 Modal Assurance Criterion

The modal assurance criterion (MAC) is a normalized number that indicates the similarity between two vectors [5]. A MAC value of zero indicates the two vectors are orthogonal, while a value of one indicates that they are identical.

Logan's work established a connection between the measured and the simulated DRCs. Thus, assuming the measured response can be represented by the simulated spectrum, it is possible to analyze the uniqueness of the design by comparing each DRC with every other possible DRC to find the worst performance. Eqn. 1 defines the MAC number as

$$MAC_{g,h,i,j} = \frac{\left(\mathbf{u}_{g,h}^T \mathbf{v}_{i,j}\right)^2}{\left(\mathbf{u}_{g,h}^T \mathbf{u}_{g,h}\right)\left(\mathbf{v}_{i,j}^T \mathbf{v}_{i,j}\right)}, \tag{1}$$

where $\mathbf{u}_{g,h}$ and $\mathbf{v}_{i,j}$ are the DRCs for the respective initial positions $(\theta = g\Delta\theta, \phi = h\Delta\phi)$ and $(\theta = i\Delta\theta, \phi = j\Delta\phi)$.

Considering all vector shifts, the maximum MAC number, which corresponds to the most similar pair of DRCs is given in Eqns. 2.

$$M = max_{g,h,i,j}\left(MAC_{g,h,i,j}\right), \tag{2}$$

where $g \neq i$ and $h \neq j$. An examination of Eqn. 2 shows that a bias in vectors $u$ and $v$ will result in a non-zero $M$ value. Thus, the DRCs are normalized such that each one is zero mean over $\theta$. These normalized DRCs form the reduced DRM or $\mathbf{DRM_{red}}$.

### 3.3 Design Methodologies

There are two general classes for the geometry creation. The first method assumes that both the initial $\theta$ and $\phi$ positions are to be identified. The second approach uses a geometric marker, which allows the initial $\theta$ location to be calculated. This assumption simplifies the $\theta$ identification and removes the $\theta$ shift effects. Both of these classes create a two dimensional matrix, which is mapped as the mask thickness to three dimensional space using spherical coordinates.

#### 3.3.1 Identifying $\theta$ and $\phi$

It is impossible to create linearly independent DRCs. So, the optimized design objective is to create a design with the least amount of linear dependence. The three following methods are tailored to create designs for identifying both $\theta$ and $\phi$ with a low linear dependence. The eigenvector approach shown in Section **??** solves a mass normalized eigenvalue problem. The binary method described in Section 3.3.2 uses patterns of ones and zeros to represent the geometry. Lastly, Hadamard approach used for rotating encoding masks was modified and applied.

#### 3.3.2 Binary Approach

The binary approach uses ones and zeros to represent the geometry thickness. Notice that the mask's cyclic nature causes vectors such as [1 1 0 0] to be the same as [1 0 0 1], where the first vector is the second shifted by one entry to the right. If the design uses binary patterns such as these two, the DRCs for two initial positions will be identical. For $n = 32$, there are many possible basis vectors; especially considering that the vectors can be shifted left or right (corresponding to multiplication or division by 2), and the $\phi$ vector order (1st, 2nd, 3rd, etc) may be swapped. This flexibility allows one to create unique geometries, mechanically balance the mask, or improve the likelihood of obtaining a signal given a random source position by more evenly spreading the ones and zeros around the mask.

#### 3.3.3 Decoupling $\theta$ and $\phi$

An alternative approach introduces additional material to create a low measurement "dead" zone at a consistent $\theta$ position. As a result, the initial $\theta$ position is assumed to be the angular distance difference between the start of the measurement and the minimum measurement location. As the initial $\theta$ position is known, the reference DRM angle may be

changed to the known θ position by shifting the basis matrix entries by the corresponding index number. This knowledge decouples the θ and ϕ identification, resulting in only needing to compare the measured DRC to the $m$ ϕ curves in $\mathbf{DRM}_{red}$. Using this method, it is possible to create $m$ linearly independent geometric basis vectors.

One such linearly independent basis is the Hadamard matrix, which has been used in the design of stationary encoding masks in the fields of spectrometry and imaging [6–8].

The Hadamard matrix is thought to only exist for square matrices where $n$ is 1, 2, or divisible by 4 [6]. By construction, the mask design under consideration is discretized in order to have $n = 32$. Also, a Hadamard matrix has ones and negative ones. To convert it to a binary pattern, the negative one entries were changed to zeros. In order to create the "dead" zone, the vector of ones corresponding to $\theta = 0$ were changed to twos. A normalized geometry resulted by following the same steps as outlined in the eigenvector approach.

### 3.4 Design Evaluation

To assess the design optimality, four criteria relevant to the performance of the RSM are proposed. The first, the maximum MAC value, was discussed in Section 3.2. The average MAC number, $A$, is given in Eqn. 3 and provides information about the mean linear dependence.

$$A = \frac{1}{b} \sum_{g,h,i,j} \left( MAC_{g,h,i,j} \right), \tag{3}$$

where $g \neq i$, $h \neq j$, and $b$ is the total number of combinations. For the $n = 32$ and $m = 30$ mask design, $b = 14850$. The optimal design should have low $M$ and $A$ values.

The third criteria measures the RSM's average efficiency for a mask cell. A high-efficiency design produces more accurate results in less measurement time, an important factor to consider for the intended applications of the RSM. This value is calculated as

$$\varepsilon = \frac{\sum_{i,j} \mathbf{DRM}_{red}}{n\, m}, \tag{4}$$

where $n\, m$ is the total number of mask cells.

The final evaluation criterion focuses on the design's sensitivity. The ratio of the maximum to minimum response in Eqn. 5 provides information on the relative amount of measurement time required and the measurement's sensitivity to random measurement noise.

$$S = min_j \left( \frac{max_i \left[ \mathbf{DRM}_{red} \right]}{min_i \left[ \mathbf{DRM}_{red} \right]} \right). \tag{5}$$

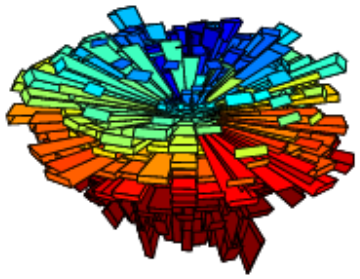

Fig. 1. RSM geometry created by the eigenvector approach.

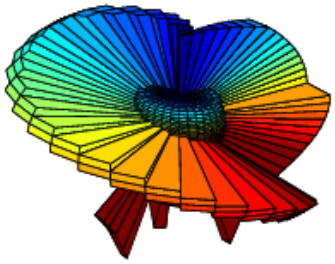

Fig. 2. RSM geometry created by the binary approach.

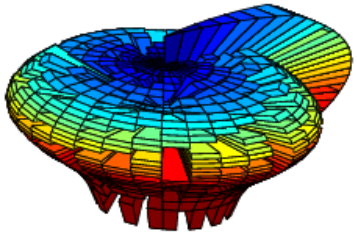

Fig. 3. RSM geometry created by the Hadamard approach.

## 4 Results and Analysis

The proposed design methodologies produced the geometries shown in Figs. 1 to 3.

The eigenvector approach used 32 $k$ values from 0.1 to -0.2999 in increments of -0.0129 with stiffness coupling to the nearest two neighbors on both sides of the mass. $c$ was determined to be 0.999 from the design surface minimization depicted in Fig **??**. Other coupled systems did not have an optimal $c$ value close to one.

The binary pattern was constructed to have a fin that spirals around the mask. As it is not possible to have the fin completely cover the mask geometry, four other vectors were added to create the necessary basis.

The FitzGerald's RSM was used as a baseline to establish the design improvement for the RSM designs shown in Figs. 1 to 3.

Table 1 summarizes the evaluation results for the original RSM, binary, eigenvector (EV), and Hadamard approaches. Recall that the Hadamard values correspond to those obtained without shifting vectors since the initial θ position can be deduced.

The proposed methods have lower $M$ values with the

Table 1. Evaluation criteria comparisons from the original design and the three proposed designs from this work.

| Criteria | Fitzgerald | EV | Binary | Hadamard |
|---|---|---|---|---|
| M | 1.00 | 0.808 | 0.963 | 0.935 |
| A | 0.210 | 0.0663 | 0.125 | 0.423 |
| $\varepsilon\left(\times 10^{-4}\right)$ | 3.75 | 2.96 | 3.86 | 3.70 |
| S | 1.00 | 1.07 | 1.16 | 1.07 |

most desirable corresponding to the eigenvector approach. The Hadamard method produces vectors which on average share 42.3% of their information, which is more than the original design. The rapid change between ones and zeros coupled with the spatial resolution limits make the Hadamard method non-ideal for this problem. The lowest average MAC number corresponds to the eigenvector approach with only 6.63% similarity. These results indicate that the method that produces the most unique DRCs is the eigenvector approach. However, the trade-off is that the eigenvector method produced a RSM with a lower average normalized number of counts per cell. The binary method has the most average normalized number of counts per cell, but also the highest sensitivity. This high sensitivity may indicate that certain initial positions are more susceptible to measurement noise.

## References


[1] J. G. M. FitzGerald, A rotating scatter mask for inexpensive gamma-ray imaging in orphan source search: Simulation results, IEEE Transactions on Nuclear Science 62 (1) (2015) 340–348. doi:10.1109/TNS.2014.2379332.

[2] J. Logan, D. Holland, L. Burggraf, J. Clinton, B. ODay, Monte carlo analysis of a novel directional rotating scatter mask photon detection system, IEEE Transactions on Nuclear Science 0 (submitted).

[3] S. Agostinelli, J. Allison, K. Amako, J. Apostolakis, H. Araujo, P. Arce, M. Asai, D. Axen, S. Banerjee, G. Barrand, F. Behner, L. Bellagamba, J. Boudreau, L. Broglia, A. Brunengo, H. Burkhardt, S. Chauvie, J. Chuma, R. Chytracek, G. Cooperman, G. Cosmo, P. Degtyarenko, A. Dell'Acqua, G. Depaola, D. Dietrich, R. Enami, A. Feliciello, C. Ferguson, H. Fesefeldt, G. Folger, F. Foppiano, A. Forti, S. Garelli, S. Giani, R. Giannitrapani, D. Gibin, J. G. Cadenas, I. Gonzlez, G. G. Abril, G. Greeniaus, W. Greiner, V. Grichine, A. Grossheim, S. Guatelli, P. Gumplinger, R. Hamatsu, K. Hashimoto, H. Hasui, A. Heikkinen, A. Howard, V. Ivanchenko, A. Johnson, F. Jones, J. Kallenbach, N. Kanaya, M. Kawabata, Y. Kawabata, M. Kawaguti, S. Kelner, P. Kent, A. Kimura, T. Kodama, R. Kokoulin, M. Kossov, H. Kurashige, E. Lamanna, T. Lampn, V. Lara, V. Lefebure, F. Lei, M. Liendl, W. Lockman, F. Longo, S. Magni, M. Maire, E. Medernach, K. Minamimoto, P. M. de Freitas, Y. Morita, K. Murakami, M. Nagamatu, R. Nartallo, P. Nieminen, T. Nishimura, K. Ohtsubo, M. Okamura, S. O'Neale, Y. Oohata, K. Paech, J. Perl, A. Pfeiffer, M. Pia, F. Ranjard, A. Rybin, S. Sadilov, E. D. Salvo, G. Santin, T. Sasaki, N. Savvas, Y. Sawada, S. Scherer, S. Sei, V. Sirotenko, D. Smith, N. Starkov, H. Stoecker, J. Sulkimo, M. Takahata, S. Tanaka, E. Tcherniaev, E. S. Tehrani, M. Tropeano, P. Truscott, H. Uno, L. Urban, P. Urban, M. Verderi, A. Walkden, W. Wander, H. Weber, J. Wellisch, T. Wenaus, D. Williams, D. Wright, T. Yamada, H. Yoshida, D. Zschiesche, Geant4a simulation toolkit, Nuclear Instruments and Methods in Physics Research Section A: Accelerators, Spectrometers, Detectors and Associated Equipment 506 (3) (2003) 250 – 303. doi:https://doi.org/10.1016/S0168-9002(03)01368-8.
URL http://www.sciencedirect.com/science/article/

[4] J. T. Goorley, M. R. James, T. E. Booth, F. B. Brown, J. S. Bull, L. J. Cox, J. W. Durkee Jr, J. S. Elson, M. L. Fensin, R. A. Forster III, et al., Initial mcnp6 release overview-mcnp6 version 1.0, Tech. rep., Los Alamos National Laboratory (LANL) (2013).

[5] R. J. Allemang, The modal assurance criterion twenty years of use and abuse, Sound and Vibration (2003) 14–21.

[6] N. Sloane, M. Harwit, Masks for hadamard transform optics, and weighing designs, Applied Optics 15 (1).

[7] S. A. Dyer, Hadamard transform spectrometry, Chemometrics and Intelligent Laboratory Systems 12 (2) (1991) 101 – 115. doi:https://doi.org/10.1016/0169-7439(91)80119-B.
URL http://www.sciencedirect.com/science/article/

[8] M. H. Finger, T. A. Prince, Hexagonal uniformly redundant arrays for coded-aperture imaging, Tech. rep., NASA Astrophysics Data System (1985).